Rail Flatness Measurement Based on Dual Laser Triangulation

Rubén Usamentiaga, *Senior Member, IEEE*, Daniel F. Garcia, and Francisco J. delaCalle

***Abstract*—Surface metrology is crucial task in automated quality control. The measurement of surface features such as regular and irregular patterns, roughness, waviness, flatness and dimensions is of utmost importance to ensure products are being manufactured according to specifications. This work focuses on flatness measurement in rails, which is a quality parameter affected by roller deformations during rail production. This work proposes a flatness measurement system for rails based on a dual triangulation configuration. Innovative solutions are provided for the most challenging tasks including calibration, registration, calculation of the deviations of the surface from their intended shape, filtering and flatness characterization. Extensive tests on synthetic and real data indicate excellent performance in terms of measurement accuracy, robustness and reliability.**

***Index Terms*—Flatness measurement, surface inspection, surface metrology.**

I. Introduction

AUTOMATED vision-based inspection systems have become very popular in recent decades due to the low maintenance and high efficiency of the technology [2]. Nowadays, the technology is mature and widely accepted in the metal industry. Not long ago, it was quite common to manually assess the quality of the metal products. A trained technician would select a random piece of the product and inspect the shape looking for defects or anomalies. The procedure was very time-consuming, slow and prone to errors due to fatigue. Moreover, only a small portion of the production could be inspected. Therefore, manual quality inspection has been gradually substituted by automated solutions. Vision-based techniques now play a vital role in quality control in the metal industry.

Flatness is a key geometrical feature used to estimate the quality of metal products. Roller thermoelastic deformations during production are the most common cause of flatness defects in metal products. Flatness measurement methods are required to ensure compliance with quality criteria before the manufactured products are used. Particularly, flatness defects in rails increase vibrations, affecting the comfort of passengers and the stability of trains [3], particularly in high-speed railways. These defects could even affect the safety of the rail line. The area most affected by flatness defects is the head of the rail. This area is critical, as it is where the wheel is in contact with the rail. A graphical representation of these defects can be seen in Fig. 1. Flatness defects can be periodical. In these cases, they can be analyzed in terms of wavelength periods, expressed in meter per cycle, and amplitudes.

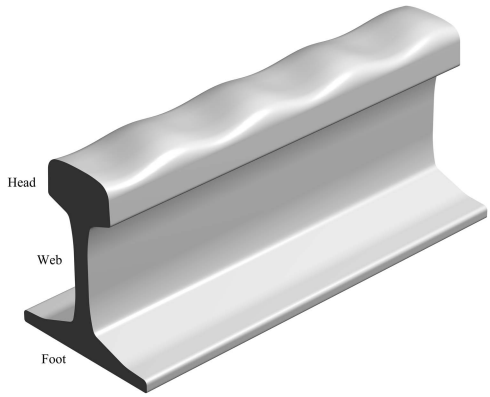

Fig. 1. Rail with flatness defects in the head area.

Flatness measurement is described in different international standards. For Europe, the standard EN-13674-1 is used [4]. In accordance with this international standard, the rail is divided into different parts: rail front, rail end, overlap and body. In each part, different flat tools (rulers), each with a specific length, are placed on the rail. Then, a technician measures the depth of the resulting valley between the support points of the rule. This time-consuming operation is repeated by moving the rule along the length of the rail. The whole operation must be repeated using rules of different lengths. Thus, manual flatness measurement is not a viable option for online monitoring and control. Nowadays, non-contact methods are the most common solution for rail flatness measurement and characterization.

Inspection methods based on structured light systems are the most common technology to measure flatness in rail mills [5]. These systems are composed of a laser projector and an industrial camera, which form a triangulation unit. The laser light projected on the rail forms a distinguishable laser stripe that shows the

Manuscript received 7 December 2023; revised 15 February 2024; accepted 4 March 2024. Date of publication 12 March 2024; date of current version 22 July 2024. Paper 2023-METC-1868.R1, presented at the 2023 IEEE Industry Applications Society Annual Meeting, Nashville, TN, USA, Oct. 29–Nov. 02, and approved for publication in the IEEE Transactions on Industry Applications by the Metal Industry Committee of the IEEE Industry Applications Society [DOI: 10.1109/IAS54024.2023.10406938]. This work was supported by the Spanish National Plan for Research, Development and Innovation under Grant PID2021-124383OB-I00. An earlier version of the paper was presented at the IEEE IAS Annual Meeting 2023 in Nashville [DOI: 10.1109/IAS54024.2023.10406938]. *(Corresponding author: Rubén Usamentiaga.)*

The authors are with the Department of Computer Science, Engineering, University of Oviedo, 33204 Gijón, Spain (e-mail: rusamentiaga@uniovi.es; dfgarcia@uniovi.es; delacalle@uniovi.es).

Color versions of one or more figures in this article are available at https://doi.org/10.1109/TIA.2024.3376322.

Digital Object Identifier 10.1109/TIA.2024.3376322

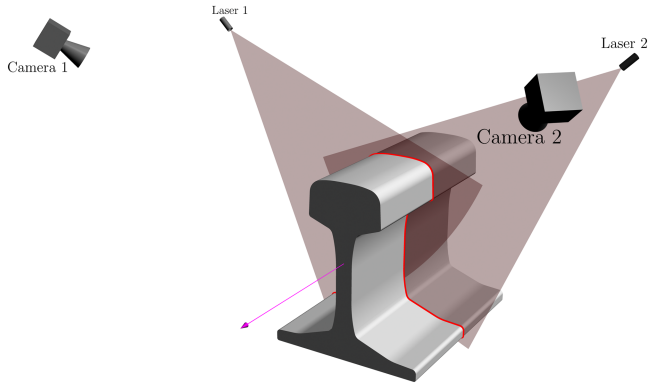

Fig. 2. Architecture of the system with two cameras and two corresponding laser projectors.

geometric features of the shape. This laser stripe is extracted from the image captured by the camera, resulting in a height profile with a cross-section of the rail [6]. A system to measure flatness following this principle is presented in [7] using two triangulation units and in [8] using five. In this work, a series of triangulation units are installed along the length of the rail. Then, the height at each position is combined to determine a height profile along the rail. Flatness features are extracted from this profile. The presented methods prevent vibrations from affecting flatness measurement. However, they result in complex systems that require multiple cameras and laser projectors, resulting in a difficult maintenance with high cost. Different solutions using a single triangulation unit have also been presented, such as [9]. In this case, three laser projectors parallel to the rail are used. Thus, a single triangulation unit extracts the height profile along the rail. This architecture is not very common, as it could be affected by vibrations and displacements of the rail during manufacturing, making it very difficult to trace the center line of the rail head.

Simplified solutions have also been presented without laser projectors. Examples of such systems can be found in [10] and [11]. In these systems, images are processed to extract the rail surface by calculating the position of the edges in the head. Then, features from this area are used to estimate the rail flatness wavelength period using the FFT. The resulting architecture is easier to implement than a triangulation unit. However, these inspection systems are very sensitive to illumination changes and the reflective properties of the rail surface, which is a major issue in industrial environments.

Due to the limitations of the available systems,this work proposes a flatness measurement system for rails based on a dual triangulation configuration, where two triangulation units are used. The proposed system observes the rail head from both the left and the right using these triangulation units, avoiding occlusions and providing a complete cross section of the area, as can be seen in Fig. 2. The resulting profile is aligned to the model to compensate for vibrations using different steps. The process is used to prevent vibrations from affecting measurements. Then distance deviations from the aligned profile to the model are calculated and filtered to measure flatness. The proposed system, which only requires two triangulation units, is not sensitive to changes in illumination and robust under vibrations during manufacturing. Moreover, this work proposes a calibration procedure that can be applied to the two triangulation units at the same time using a simple flat calibration target, greatly simplifying maintenance.

This article is organized as follows: Section II presents the proposed approach for the flatness measurement system; Section III discusses the results obtained, and finally, Section IV reports conclusions.

II. Proposed Approach

The proposed approach is based on two cameras and the two corresponding laser projectors to measure the coordinates of a cross-section around the top area of the rail. The resulting sets of image coordinates are translated into world units and combined into a single profile using an accurate calibration procedure. Then, the profile is aligned using a combination of global and local registrations. Finally, the deviations are filtered, and flatness features are extracted and analyzed to provide quality metrics.

A. Calibration

The predominant method for camera calibration involves utilizing a known calibration object to determine both internal and external camera parameters. This is achieved by establishing correspondences between points on the calibration object and their counterparts in captured images [12]. While this approach offers simplicity and typically yields high calibration accuracy, its effectiveness is heavily reliant on the precision of the calibration object.

Alternatively, self-calibration methods exist wherein camera parameters are estimated without the need for high-precision calibration objects [13]. These techniques leverage geometric structures such as lines and vanishing points to model the 3D-2D correspondence within the scene. While offering greater flexibility, this approach tends to sacrifice some accuracy and robustness compared to traditional methods.

Recent trends in camera calibration have seen a notable uptake in the adoption of deep learning techniques [14], [15]. These approaches involve training neural networks on extensive datasets of images annotated with ground truth calibration parameters. Through this process, the networks can effectively discern intricate relationships between image characteristics and camera parameters. Such innovative techniques hold promise for facilitating real-time calibration and adaptation to dynamic environmental conditions. The incorporation of deep learning into camera calibration presents a compelling avenue for enhancing accuracy, flexibility, and automation compared to conventional methods. However, in industrial environments, where reliability and robustness are paramount, challenges persist.

1) Camera Model: Measurements using a camera require the transformation from image to world coordinates. The geometric model for the projection of world coordinates in the scene onto the image is the pinhole model, which is represented in Fig. 3.

A point $P^w = (x^w, y^w, z^w)^T$ in world coordinates is transformed into pixel coordinates $(c, r)^T$ using a series of geometric

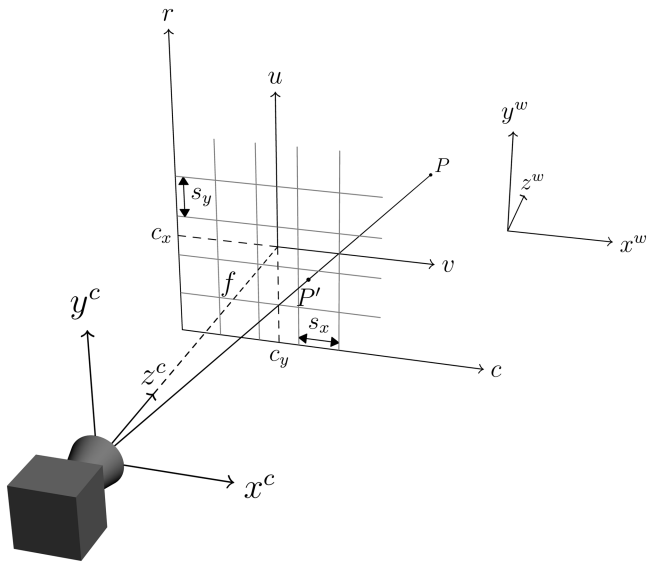

Fig. 3. Camera model.

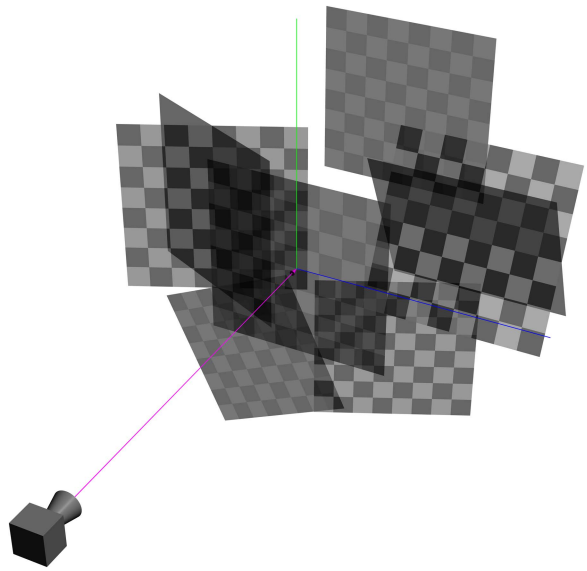

Fig. 4. Intrinsic calibration using a planar calibration target observed by the camera from different orientations.

transformations. First, a 3D rigid-body transformation from world coordinates in the scene to camera coordinates is applied. This transformation assumes the camera z-axis is perpendicular to the image plane. A 3D rigid-body transformation is defined using three rotations (α, β, γ) and three translations (t_x, t_y, t_z). These parameters are referred to as extrinsic camera parameters and describe the position and orientation of the camera with respect to the world reference system. The rigid transformation can be expressed as (1), where $P^w = (x^w, y^w, z^w)^T$ and $P^c = (x^c, y^c, z^c)^T$ represent the points in world and camera coordinates, and r_{ij} are obtained from the rotation angles.

$$\begin{pmatrix} x^c \\ y^c \\ z^c \\ 1 \end{pmatrix} = \begin{pmatrix} r_{11} & r_{12} & r_{13} & t_x \\ r_{21} & r_{22} & r_{23} & t_y \\ r_{31} & r_{32} & r_{33} & t_z \\ 0 & 0 & 0 & 1 \end{pmatrix} \begin{pmatrix} x^w \\ y^w \\ z^w \\ 1 \end{pmatrix} \tag{1}$$

The rigid transformation can also be expressed as (2), where $H_{w \to c}$ represents the transformation from the world to the camera.

$$\begin{pmatrix} P^c \\ 1 \end{pmatrix} = H_{w \to c} \begin{pmatrix} P^w \\ 1 \end{pmatrix} \tag{2}$$

The second transformation performs a perspective projection from camera coordinates to the image plane. This transformation can be expressed as (3), where $(u, v)^T$ is the corresponding point in the image plane coordinate system. This transformation depends on f, the focal length.

$$\begin{pmatrix} u \\ v \\ 1 \end{pmatrix} = \begin{pmatrix} f & 0 & 0 & 0 \\ 0 & f & 0 & 0 \\ 0 & 0 & 1 & 0 \end{pmatrix} \begin{pmatrix} x^c \\ y^c \\ z^c \\ 1 \end{pmatrix} \tag{3}$$

The third transformation is a 2D affine transformation from image plane coordinates to pixel coordinates. This transformation can be expressed as (4), where $(c, r)^T$ are the column and row of the pixel. This transformation depends on the size of the pixels $(s_x$ and $s_y)$ and the position of the center in the image $(c_x$ and $c_y)$.

$$\begin{pmatrix} c \\ r \\ 1 \end{pmatrix} = \begin{pmatrix} \frac{1}{s_x} & 0 & c_x \\ 0 & \frac{1}{s_y} & c_y \\ 0 & 0 & 1 \end{pmatrix} \begin{pmatrix} u \\ v \\ 1 \end{pmatrix} \tag{4}$$

A final non-linear correction is usually applied to compensate for optical distortions, which can be expressed as (5), where $a_c = (c, r)^T$ represents the correct coordinates, $a_d = (c', r')^T$ the distorted coordinates, $\mathcal{F}$ is a nonlinear distortion function, and δ represents a set of coefficients that describe distortion.

$$a_c = a_d + \mathcal{F}(a_d, \delta) \tag{5}$$

The parameters that control the transformation from camera to pixel coordinates are referred to as intrinsic camera parameters. Therefore, there are two types of parameters that control the transformation from world to pixels coordinates: intrinsic and extrinsic parameters. The estimation of these two sets of parameters requires two different calibration procedures: intrinsic calibration and extrinsic calibration.

2) Intrinsic Calibration: The intrinsic calibration proposed in this work follows the method proposed by [16]. In this method, a planar calibration target with a checker pattern is observed by the camera from different orientations to obtain multiple correspondences, as can be seen in Fig. 4. For each observation, a linear approximation is applied to obtain an initial guess of the projection parameters. Then, an iterative algorithm is used to optimize the estimation considering all the data.

Nowadays, the intrinsic calibration method is readily available in many software packages and tools. Thus, it is a straightforward procedure. This calibration procedure must be applied to each of the two cameras used in the inspection system. The intrinsic calibration only needs to be performed once unless the camera lens is changed. Moreover, it can be performed in a laboratory with a controlled environment. Additional sources

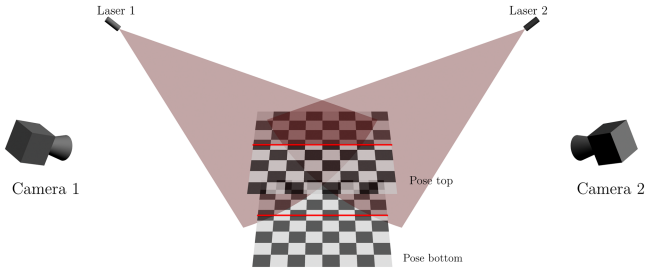

Fig. 5. Extrinsic calibration using a planar calibration target and two poses to calculate the laser plane.

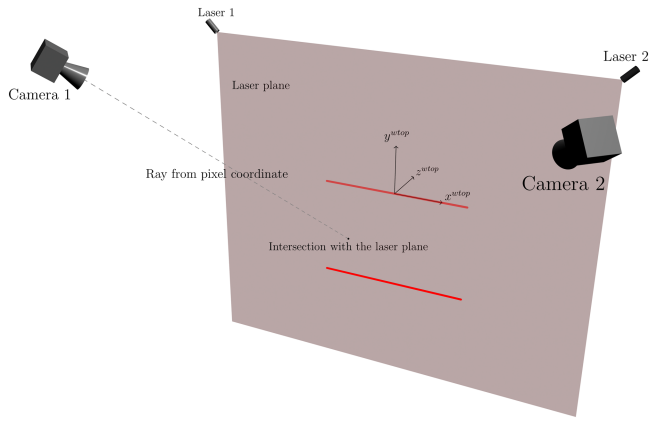

Fig. 6. Fitting the laser plane using the coordinates of the laser strips.

of error during calibration, such as temperature fluctuations or mechanical deterioration or the calibration plate are considered negligible.

3) Extrinsic Calibration: The extrinsic calibration is used to calculate the position and orientation of the camera with respect to the world reference systems. Thus, it must be performed in the industrial plant where the inspection system is installed, increasing the complexity of the procedure.

The camera model maps 3D points in world coordinates to 2D pixel coordinates. However, the inverse transformation is undefined, as multiple 3D points correspond to the same 2D pixel coordinates. In order to perform measurements with a camera, a measurement plane in world coordinates needs to be defined. Then, the inverse transformation is defined as the intersection of the optical ray starting from the pixel coordinate, with the measurement plane. Measurements using laser triangulation define the measurement plane as the plane built by the projection of the laser light onto the inspected object, i.e., the laser plane.

The proposed approach to estimate the position of the laser plane is based on the same planar calibration target. The calibration target is placed in two positions: top and bottom, as can be seen in Fig. 5, although the positions do not need to be parallel. It must be placed in the field of view of the two cameras and intersecting the laser plane. For each position, two images are acquired from camera 1 and another two from camera 2. The first image is acquired when the laser projector is turned off, i.e., observing the calibration target, and the second with the laser stripe projected on the calibration target. The information of the first image is used to estimate the homography that describes the rigid transformation from world coordinates in the planar pattern to each camera coordinate. Thus, the transformations $H_{wtop\rightarrow c1}$ and $H_{wtop\rightarrow c2}$ are calculated. Similarly, $H_{wbot\rightarrow c1}$ and $H_{wbot\rightarrow c2}$ are calculated when the calibration target is placed at the bottom position.

A rigid transformation is invertible. Thus, the transformations from the camera coordinate systems to the world can be calculated using (6), (7), (8), (9).

$$H_{c1\rightarrow wtop} = (H_{wtop\rightarrow c1})^{-1} \tag{6}$$

$$H_{c2\rightarrow wtop} = (H_{wtop\rightarrow c2})^{-1} \tag{7}$$

$$H_{c1\rightarrow wbot} = (H_{wbot\rightarrow c1})^{-1} \tag{8}$$

$$H_{c2\rightarrow wbot} = (H_{wbot\rightarrow c2})^{-1} \tag{9}$$

These transformations can be also combined to obtain the transformation from one position to the other, which can expressed as (10) or (11).

$$H_{wtop\rightarrow wbot} = H_{c1\rightarrow wbot} H_{wtop\rightarrow c1} \tag{10}$$

$$H_{wtop\rightarrow wbot} = H_{c2\rightarrow wbot} H_{wtop\rightarrow c2} \tag{11}$$

The images acquired with the two cameras when the laser is projected on the calibration target are processed to extract the image coordinates of the laser stripes. The image coordinates at the top position are translated to world coordinates using $H_{c1\rightarrow wtop}$ and $H_{c2\rightarrow wtop}$, respectively for each camera. The same approach is used for the image coordinates at the bottom position using $H_{c1\rightarrow wbot}$ and $H_{c2\rightarrow wbot}$. The coordinates in $wbot$ are then translated to $wtop$. The results are sets of coordinates of the two laser stripes in the same world reference system. These coordinates are used to fit a plane that provides the coordinates of the laser plane, i.e., the measurement plane.

The proposed approach solves the extrinsic calibration problem because now the inverse transformation from camera to world coordinates is possible, as the intersections from rays starting from pixel coordinate with the laser plane can be calculated. This intersection is represented in Fig. 6. The proposed approach provides a simple yet accurate extrinsic calibration method, suitable for application in industrial environments.

B. Registration

The inspection procedure acquires images from the laser projected on the surface on the rail. The pixel coordinates are then extracted from the images using the method proposed in [17] and transformed into world coordinates following the estimated model of the camera with the calibration procedure. The result is a profile with a cross-section of the head of the rail. However, in order to determine geometrical features from this profile, it first needs to be aligned with the geometrical model of the inspected product, in this case the rail. This alignment procedure is generally referred to as registration.

The primary point cloud registration algorithms are typically grouped into three main categories: optimization-based, feature-based, and end-to-end-based approaches. Optimization-based

methods often rely on the Iterative Closest Point (ICP) algorithm, a widely used technique that iteratively refines a rigid transformation to align two point clouds by iteratively finding the closest points and updating the transformation parameters [18]. Feature-based approaches, on the other hand, focus on identifying distinctive features within point clouds, such as keypoints or local descriptors, to establish correspondences between them. End-to-end-based approaches leverage deep learning techniques to directly learn the transformation between point clouds, thus bypassing the need for explicit correspondence finding and transformation estimation steps. ICP and its variants are fundamental techniques for rigid registration between two point sets, typically yielding robust results when provided with a good initial solution and effective outlier filtering. However, algorithms like Coherent Point Drift (CPD) have been developed to address some of ICP's limitations [19], offering improved robustness to noise, outliers, and missing points, albeit at the expense of slower computational performance. End-to-end-based approaches utilizing deep learning techniques can provide advantages in certain scenarios by circumventing the explicit correspondence finding and transformation estimation steps [20]. However, the effectiveness of these methods may vary depending on the specific characteristics of the data and the complexity of the registration task.

In this work, the proposed registration procedure is divided into three consecutive steps: initial registration, global registration and local registration. The proposed initial registration provides a coarse alignment using two global features: the centroid and the orientation. The centroid is calculated as the average position of all the points in the profile and the orientation is calculated using the eigenvector with the largest eigenvalue of the covariance matrix of the profile (principal component). These two features are used to align the profile and the model: the profile is translated according to the distance between the centroids and is then rotated in function of the angle difference between the orientation of the profile and the orientation of the model. This provides a coarse alignment that is required for the next steps.

The second step in the registration process is the global registration. In this case, the profile is aligned with the model of the rail using the iterative closest point fit (ICP) algorithm. Considering the acquired profile is formed by a set of n points $\mathcal{P} = \{p_1, p_2, \ldots, p_n\}$, the goal is to find the optimal rigid transformation (R and t) that minimizes E, defined as (12), where M is the rail model and d is the Euclidean distance.

$$E = \sum_{i=1}^{n} d\left(M, \mathcal{P}R + t\right)^2 \tag{12}$$

The ICP algorithm repeats the following steps until convergence:

1) The algorithm estimates point correspondences between the profile and the model of the rail by searching for the closest point in the model to each point in the profile, where the model is defined analytically in terms of segments and arcs. For all points in the profile the correspondences $\mathcal{Q} = \{q_1, q_2, \ldots, q_n\}$ are calculated.

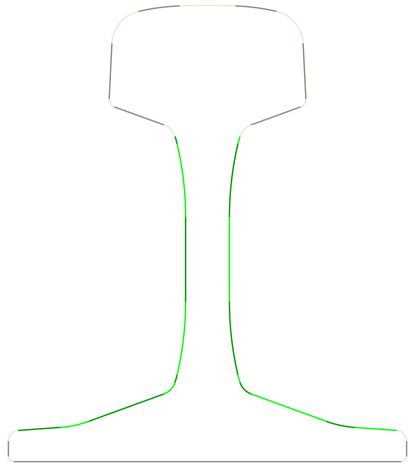

Fig. 7. Partial model used for the local robust registration.

2) The rigid transformation at iteration j (R_j and t_j) that maps $\mathcal{P}$ onto $\mathcal{Q}$ requires minimizing E_j, using the least squares error criterion (13). This problem can be efficiently solved using the mathematical procedure described in [21].

$$E_j = \sum_{i=1}^{n} |\mathcal{Q} - \mathcal{P}R_j - t_j|^2 \tag{13}$$

3) $\mathcal{P}$ is transformed according to the calculated rigid transformation using (14).

$$\mathcal{P} = \mathcal{P}R_j + t_j \tag{14}$$

The ICP algorithm improves the putative correspondences and monotonically converges to a global solution of the problem when the initial coarse registration is applied first. However, it is sensitive to noise and outliers. Moreover, flatness defects in the head can greatly affect the registration result. Therefore, the result of global registration is not suitable for the measurement of flatness. The proposed solution in this work is to apply a third registration step: the local robust registration.

The local robust registration is based on the ICP algorithm with two important modifications. First, a partial model of the rail is used. A new geometric model is created including only the geometric primitives in the web area (central part) and the top of the foot of the rail. Thus, the area affected by flatness defects is not included in the model. Fig. 7 show the partial model used (in green).

The area of the rail in the partial model is not affected by flatness defects. However, measurement noise can still be present, preventing an accurate registration. Therefore, an additional modification for the ICP is proposed: the correspondences in $\mathcal{Q}$ are filtered based on robust statistics. The distance between the potential correspondences is calculated (ε_i). Then, the median absolute deviation of these residuals is calculated using (15). Considering noise to follow a Gaussian distribution, a threshold of value 5 can be selected that contains more than 99.9% of the distribution. This effectively removes outlier correspondences. The influence of Gaussian noise on the rail profile during this

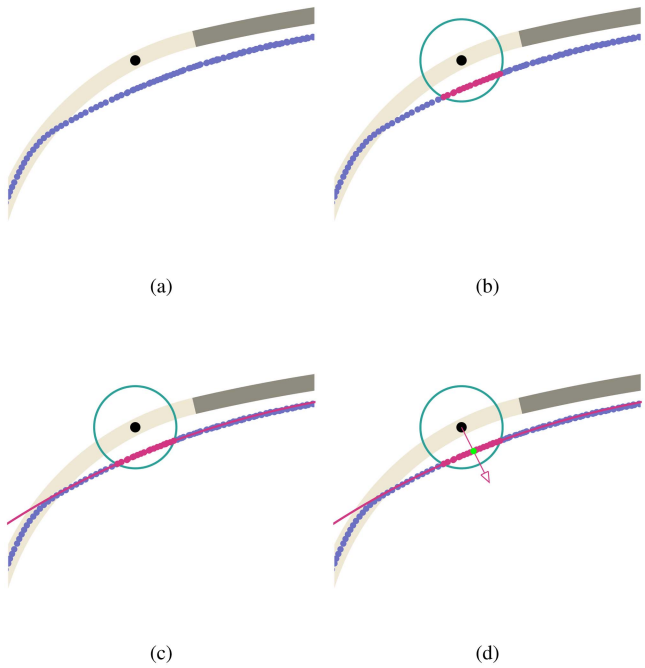

Fig. 8. Calculation of deviations from the geometric model to the profile. (a) Model and profile. (b) Close points in the profile given a radius distance. (c) Parabola fit. (d) Intersection of parabola and normal to the model.

registration is minimized using the least square criterion.

$$\mathrm{MAD} = \mathrm{median}_i \left(\left| \varepsilon_i - \mathrm{median}_j(\varepsilon_j) \right| \right) \tag{15}$$

C. Deviations From Model

Flatness is mathematically defined as the degree to which a surface approximates a plane. However, when flatness is applied to rails in curved areas, the shape of the rail model must be removed from the profile. Thus, it is necessary to calculate the deviations from the measured rail profile to the model. Only then can flatness be correctly analyzed.

The problem for the calculation of the distance deviations from the geometric model to the profile starts with the aligned profile. A partial example can be seen in Fig. 8(a). In this case, the profile is deviated downwards from the model in the head of the rail. The objective is to calculate the distance from any point in the model to the profile. In order to calculate this distance, a K-D tree with all the points of the profile is created. This data structure organizes points in space, enabling fast close-point calculations. Using this tree and given a point in the model, the closest points in the profile given a radius distance are efficiently determined. The result can be seen in Fig. 8(b). The set of points closest to the considered distance are then used to fit a parabola defined by (16). To fit the parabola, points must be rotated according to the orientation. The result is a parabola that robustly fits the profile close to the model for any given point, as can be seen in Fig. 8(c). The last step calculates the intersection between the parabola and the normal to the rail surface for the considered point. The distance from this intersection to the model is the deviation of the profile at this position.

$$y = ax^2 + bx + c \tag{16}$$

D. Filtering

In order to analyze flatness, the deviations for a region of the profile need to be calculated. In the case of flatness, the part of interest is the head. The proposed approach is to sample the geometric primitives corresponding to the region of interest at a particular resolution. Then, for any point in this discrete version of the model, the deviation to the profile can be estimated using the previous procedure. The resulting deviations do not depend on the resolution of the profile. Moreover, the resulting number of distances is always the same, which simplifies further processing and analysis. The calculated deviations are finally used to analyze flatness and extract different possible metrics.

When surface metrology is applied in automated quality inspection, specific topographic features can be measured, analyzed or filtered. The most common are roughness, waviness and form, which is the long-range deviation. The form in the proposed system is removed when deviations from the model are calculated, so a form removal driven by the geometric model is performed. The resulting deviations combine roughness and waviness. Thus, before the calculation of flatness features from the measurements, an additional step is required: filtering. The goal of the filtering procedure is to reduce and/or remove undesired information from data. In this case, the goal is to separate the waviness that provides relevant information of the flatness from the noise and roughness.

In this work, a low-pass spline filter is used to extract the waviness from the deviations, filtering roughness and noise. The spline filter provides superior performance to other filters used in surface metrology, such as the Gaussian filter [22]. This filter is based on cubic splines, which are used to smoothly link a series of points given a cutoff wavelength. The filter substitutes the measured deviations for curves created using splines that connect the input signal using a series of springs controlled by tension parameters.

E. Flatness Characterization

The final step is the extraction of feature parameters from the surface resulting from the filtering procedure. These parameters are application dependent. In rail flatness, the most common is the use of rules, and the calculation of valleys depth between support points. Other more general approaches can be found in the literature about surface metrology. The most common parameters are related to the amplitude of the height or depth of the profile elements from the mean line, such as maximum profile peak height or maximum profile valley depth; the distance between the peaks and valleys, such as the mean peak spacing or peak count; and frequency, such as the power spectral density.

III. Results and Discussion

The proposed rail flatness measurement system was built using two cameras (Genie Teledyne Dalsa HM1400) and two laser projectors (Coherent StingRay). The laser for each camera uses a different wavelength (640 nm and 685 nm), and the corresponding camera is equipped with the matching wavelength filter. This way, one triangulation unit does not affect the other.

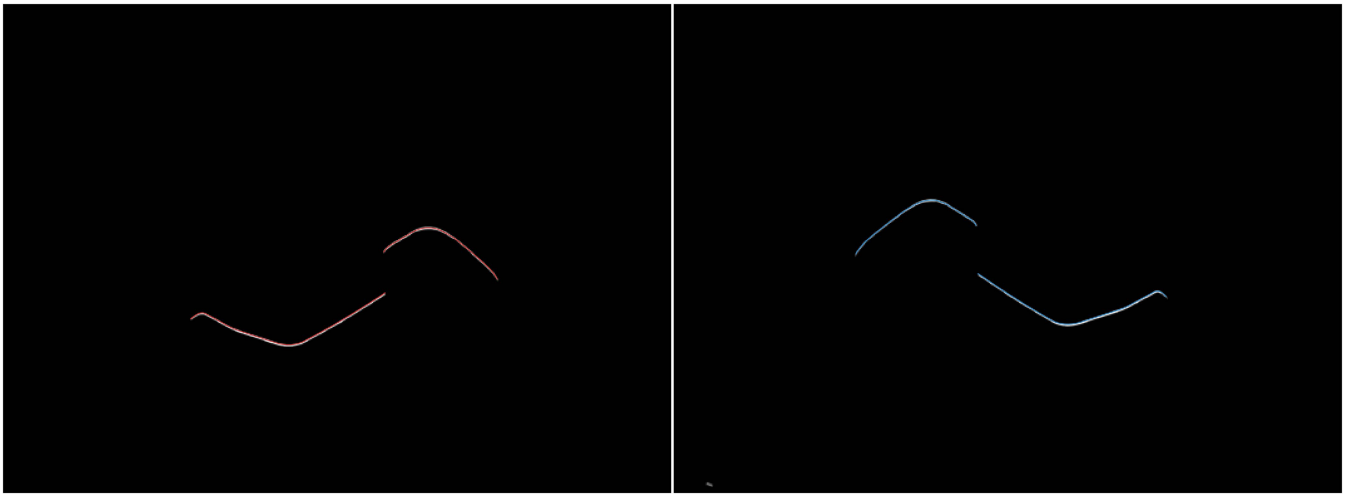

Fig. 9. Observations of the lasers projected on the rail by the two cameras. The colored lines show the calculated position of the laser stripes in the images.

A. Calibration

The intrinsic calibration is performed in a controlled environment using a planar calibration plate with a checkerboard pattern. The image coordinates of the corners of the pattern are extracted using common image processing tools. These coordinates and the well-known dimensions of the pattern are used to estimate the intrinsic camera parameters. The procedure is repeated for each of the two cameras, as they could have slightly different parameters. On average the resulting calibration accuracy expressed as the reprojection error of the image coordinates of the corners in the pattern was 0.039 mm.

The extrinsic calibration is performed using the same calibration plate. The plate is situated at two positions, following the same approach seen in Fig. 5. Thus, the extrinsic calibration for the two cameras is calculated at the same time. On average, the calibration error was 0.064 mm.

B. Registration

Using the estimated camera model, rail profiles can be measured by extracting laser coordinates in the image and performing a translation to world units. Fig. 9 shows the images observed by each camera from the laser projected on the rail surface. Given the architecture of the inspection system, each camera observes the head and one side of the rail, including the top of the foot. The images are processed to extract the laser coordinates. The colored lines in the images show the position of the extracted laser stripes. As can be seen, the system robustly detects the center of the laser stripe, providing a smooth and accurate contour. These coordinates are then translated to world units using the estimated parameters of the camera model. The result can be seen in Fig. 10.

The head area is observed by the two cameras redundantly providing more data points, thus making measurements more reliable. Fig. 11 shows a detail of the center of the head area of the profile, where the overlapping of the resulting profiles for each camera can be seen. The region is highlighted in Fig. 10. As can be seen, the measured profile is not at the center of the line corresponding to the geometric model of the rail. In this case, it is displaced slightly downwards. This is because this experiment is performed with a rail where the head has a small deviation compared with the model.

Fig. 10. Measured profile of the rail by the two cameras of the inspection system.

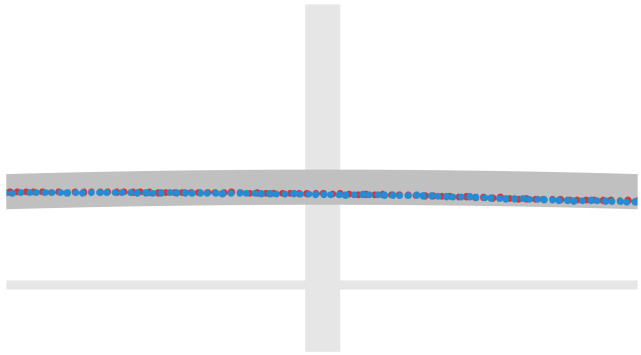

Fig. 11. Enlarged profile of the rail head observed by the two cameras.

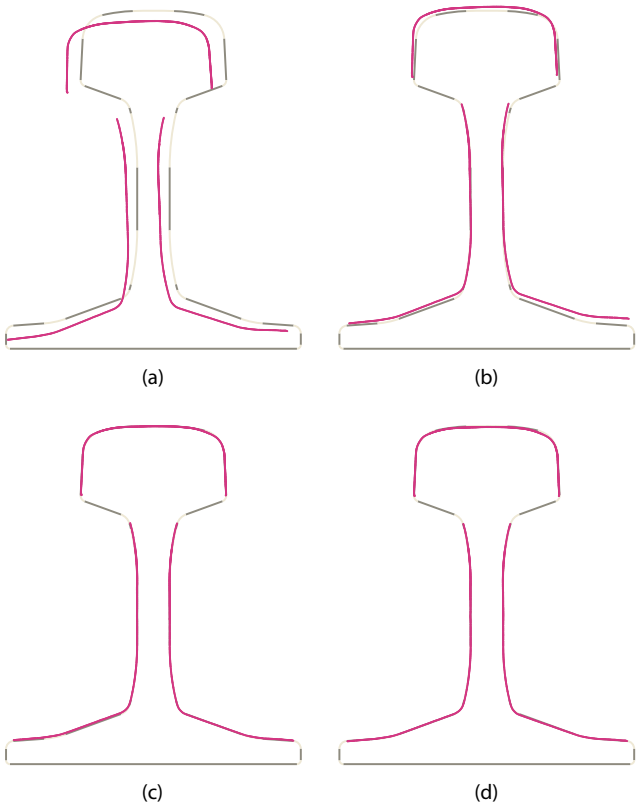

Fig. 12. Registration steps for a real rail profile. (a) Initial profile after the translation to world units. (b) Initial alignment using the centroid and orientation. (c) Global registration. (d) Local registration.

The combined profile from the two cameras requires registration with the model to calculate flatness. Fig. 12 shows the results with a real rail profile. Initially, the profile translated into world coordinates is not aligned with the model, as can be seen in Fig. 12(a). During production, the rail movement is affected by vibrations. The initial registration shown in Fig. 12(b) provides a coarse alignment. The result of the registration is required for the next step: global registration. In this step, the profile is aligned with the complete model. As can be seen in Fig. 12(c) the profile is now aligned with the model. The final registration, the local registration, accurately aligns the profile with the central part and top of the foot of the rail. The result can be seen in Fig. 12(d).

C. Synthetic Tests

The proposed approach for registration and measurements for the deviation from the model can deal with noise, outliers or flatness defects. In order to verify this statement quantitatively, synthetic tests are performed where a rail profile is corrupted with this type of issues. The accuracy for the calculation of the deviation from profile to model after registration is shown in Table I. In the experiments a random transformation that includes translations and rotations is applied to the profile. Then, the registration procedure is applied and deviations to the model are calculated. Each experiment is repeated 100 times and the results are averaged.

TABLE I
EVALUATION OF THE ACCURACY FOR THE CALCULATION OF THE DEVIATION FROM PROFILE TO MODEL USING A PROFILE CORRUPTED WITH NOISE

Experiment	Absolute average deviation (mm)
No noise	0.00033
Gaussian noise STD 0.01	0.00060
Gaussian noise STD 0.02	0.00062
Gaussian noise STD 0.05	0.00066
Gaussian noise STD 0.10	0.00068
Outliers 1%	0.00033
Outliers 10%	0.00033
Outliers 20%	0.00033
Head defect small	0.00033
Head defect large	0.00033

Tests include adding Gaussian noise to the profile with different intensities, calculated with different standard deviations. As can be seen, the proposed approach is virtually unaffected by this type of noise, producing negligible error. Also, in real applications white noise is much lower than the considered values.

Table I demonstrates the robustness of the system against outlier corruption at varying percentages. Outliers are observations in the profile that differ significantly from other observations in close proximity to the rail. The results indicate that the system is not affected by this type of noise, as it provides consistent results even with a significant number of outliers.

Tests also show what happens when there is a flatness defect in the head. In this case, the deviation is only calculated for other parts of the profile, not including the head. The results indicate that the system is effectively ignoring the head for the registration. Thus, the local registration is not considering this area for the final alignment of the profile and the model. This is essential for the calculation of deviations in this area and the subsequent flatness analysis.

The results in Table I are not zero in any experiment, not even when there is no noise. This is because the proposed procedure for the calculation of the deviation fits a portion of the profile using a quadratic function. This approach is very robust, but in very curved areas it is not able to perfectly fit the shape of the profile. nevertheless, the resulting error is negligible in all experiments.

D. Tests With Calibrated Piece

Extended tests to assess the accuracy of the registration and calculation of the deviation with respect to the model are performed using a test piece. The test piece, which can be seen in Fig. 13, contains a combination of straight lines and curves. Thus, it is a good option to assess the accuracy of the system with combined geometry. The test piece is fabricated in hard plastic using mechanical tools. Then, an industrial coordinate measuring machine with a reported accuracy of 1 μm (Renishaw Renscan) is used to accurately measure the geometry of the test piece by sensing discrete points on the surface of the object with a contact probe.

In the experiment the test piece is placed in the field of view of the two cameras at different positions. The distance from the cameras is changed to test the performance of the system

Fig. 13. Test piece during measurement in the coordinate measuring machine.

TABLE II
ACCURACY OF THE SYSTEM

Experiment	Average deviation (mm)
Intrinsic calibration	0.039
Extrinsic calibration	0.064
Test piece	0.045

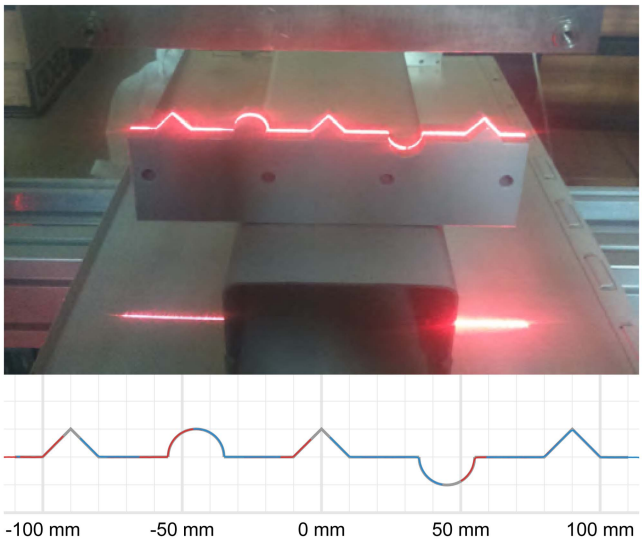

Fig. 14. Test piece with the two lasers projected and measurements.

in different conditions. During the experiment, the test piece is moved vertically: top, center and bottom. This change of position is used to simulate movement or vibrations in the rail during manufacturing.

Following the proposed inspection procedure, laser stripes are extracted and converted to world coordinates. Then, the sequence of combined profiles is aligned to the model. Finally, the deviations to the model are calculated. On average, the accuracy of the tests is 0.045 mm with a standard deviation of 0.0026 mm. This finding is comparable to the error observed in both intrinsic and extrinsic calibrations. Table II shows a summary of the accuracy results. This accuracy enables the inspection system to provide reliable flatness measurements in the most demanding environments.

Fig. 14 shows the test piece with the projection of the lasers. This figure also shows the measurements of one profile and the

Fig. 15. Coordinates of the rail measured by the system after the registration. The length of the rail has been reduced by a factor of 1000 to emphasize flatness irregularities.

geometric model. The test piece includes different geometric shapes. The proposed approach using two laser projectors placed on the top left and top right correctly illuminates the whole shape, minimizing occlusions. The combined profiles extracted from the two cameras provide the required geometric information about the shape of the piece to measure the deviations with great accuracy.

E. Tests With Rails

The proposed inspection system is installed in a rail manufacturing mill, where several flatness parameters are extracted from the head. In order to test the ability of the proposed methods to detect flatness defects, the proposed approach is applied to rails during manufacturing.

Fig. 15 shows an example of one of the inspected rails. This rail is defined in the UNE EN13674-1 standard with identification code 60E1. The figure shows the coordinates of the rail measured by the system after the registration procedure. In order to visualize flatness defects a simple yet effective approach is used in the representation: the length of the rail is reduced by a factor of 1000. This way, light in the 3D representation can be used to highlight small height variations on the surface. In this case, the perceived flatness defect in the head has a ratio period/amplitude of around 6000. This visualization makes the raw analysis very easy.

Fig. 16 shows the calculated deviations in a head area for the considered rail. Fig. 16(b) shows a 3D representation for the measured deviations along the rail length and Fig. 16(a) shows the deviations just at the center of the rail head along the rail length. The values on the Z axis in Fig. 16(b) are scaled by a factor of 10 and the length by 1/1000 to enhance the visualization. Both representations clearly show a periodic flatness defect.

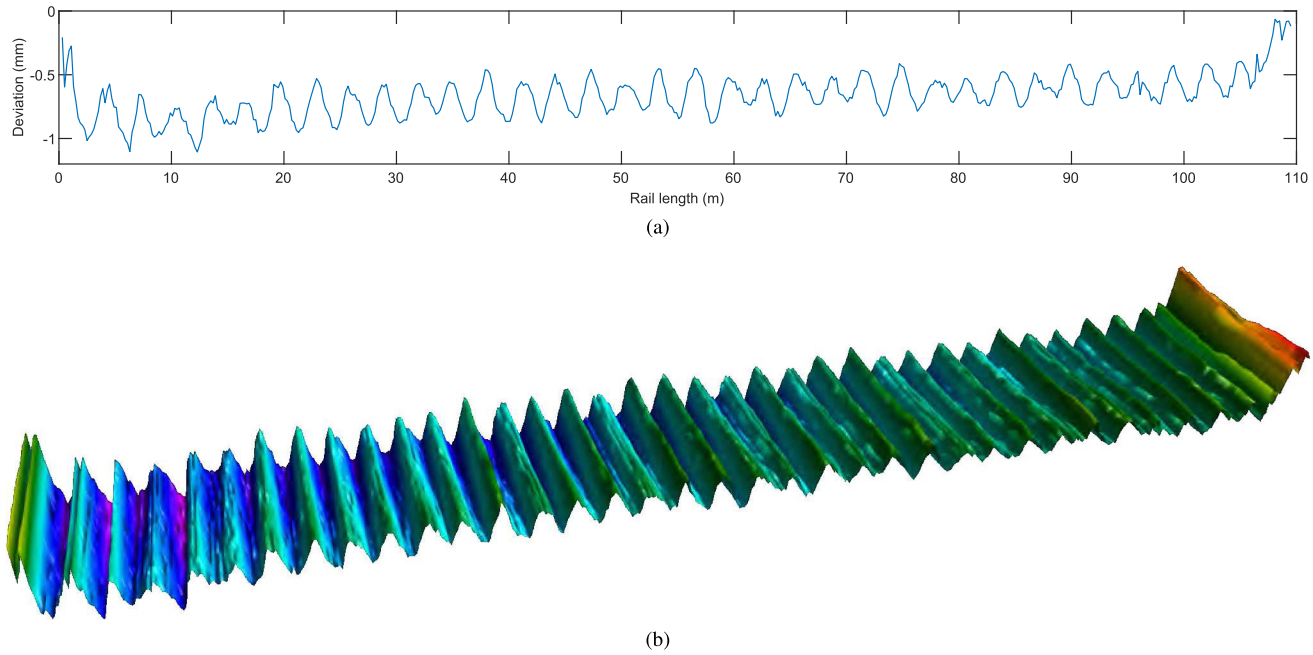

Fig. 16. Measured deviations in the head area of the rail. (a) Deviations at the center of the rail along the rail length. (b) 3D representation for the measured deviations in the head area (values on the Z axis are scaled by a factor of 10 and the length by 1/1000).

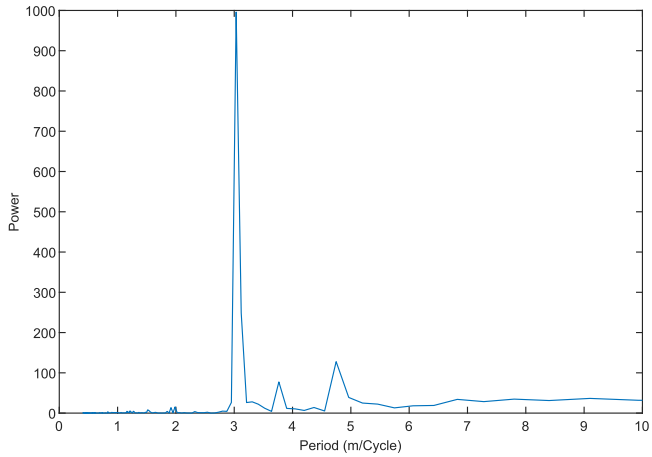

Fig. 17. Power spectrum of the deviation at the center of the head of the rail.

As can be seen in Fig. 16(a), the average amplitude is around 0.5 mm and the period is around 3 m. However, the deviations are corrupted by noise that can affect flatness characterization. In order to extract the real values of waviness the filtering approach is applied to the measured deviations.

In order to determine the correct cutoff wavelength to use in the filter, an analysis of the periodic pattern of the flatness defect is performed. Fig. 17 shows the power spectrum of the deviation at the center of the head of the rail. The peak indicates periodic wavelength of the defect. Thus, a cutoff wavelength lower than this peak can be used to remove noise from the signal.

Fig. 18 shows the resulting deviation after filtering. This figure shows the results after applying the spline filter with a cutoff wavelength of 1.75 m/cycle. As can be seen, the noise is removed, and the resulting signal provides a better representation of the flatness on the head of the rail. This filtered signal can be directly used to calculate the required flatness parameters, such as the amplitude of the height or depth of the profile elements from the mean line. The calculation of these parameters is a straightforward procedure given the filtered deviations. In this case the maximum height of the profile is 0.63 mm, the maximum profile valley depth is 0.40 mm and the period of flatness pattern is 3.03, m/cycle. These values are measured in the central part of the rail, not considering the first and last 3 meters. These parameters correctly characterize the flatness of the rail in the head area. The calculation of these parameters follows the indications of the American Society of Mechanical Engineers (ASME B46.1-2002).

F. Repeatability Tests

Repeatability tests are used to evaluate how repeatable the results are under a set of similar conditions. These experiments are performed using the same methods and algorithms; the same operator; the same equipment, the same cameras laser projectors; the same environmental conditions; the same location, the industrial installation where the system is installed; and the same item or unit under test, a rail selected from production. The tests follow the specifications in ISO 5725-1:1994.

In this experiment one rail is inspected five times. During each of these repeated inspections, the deviations in the head of the rail are calculated, and a profile is extracted at the center of the area. The resulting profiles for each inspection are shown in Fig. 19. A qualitative assessment of the resulting profiles indicates great repeatability, i,e, the results are very similar in all repetitions. The profiles also show how the largest deviations from the model

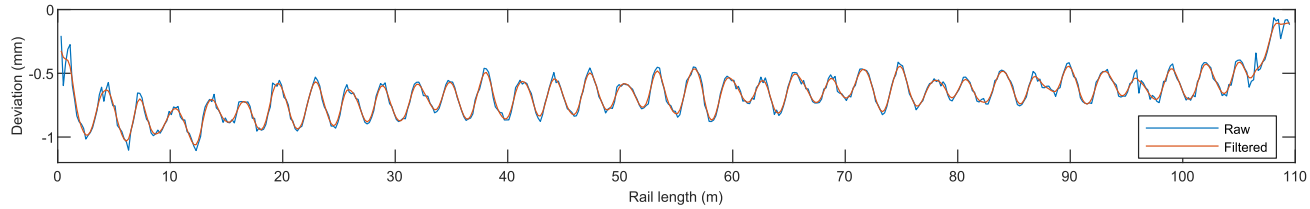

(a)

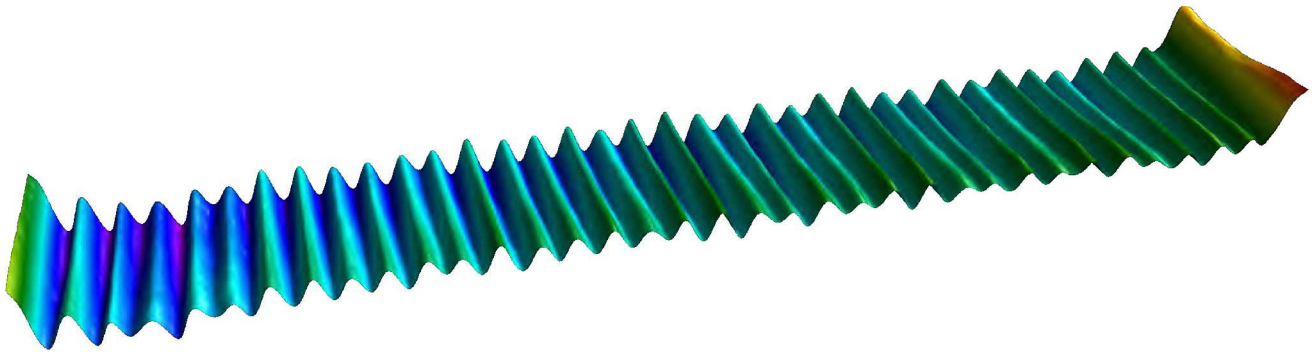

(b)

Fig. 18. Measured deviations in the head area of the rail after applying the spline filter with a cutoff wavelength of 1.75 m/cycle. (a) Deviations at the center of the rail along the rail length and filter result. (b) 3D representation for the measured deviations in the head area (values in the Z axis are scaled by a factor of 10).

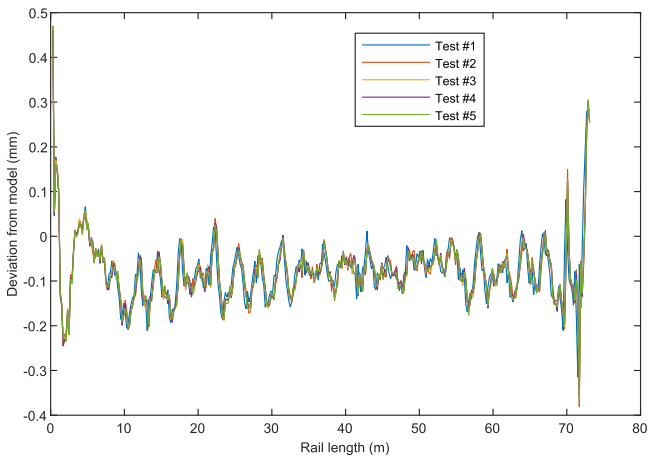

Fig. 19. Measurements of deviations from the model at the center of the rail head. The profile is measured five times to assess the repeatability of the system.

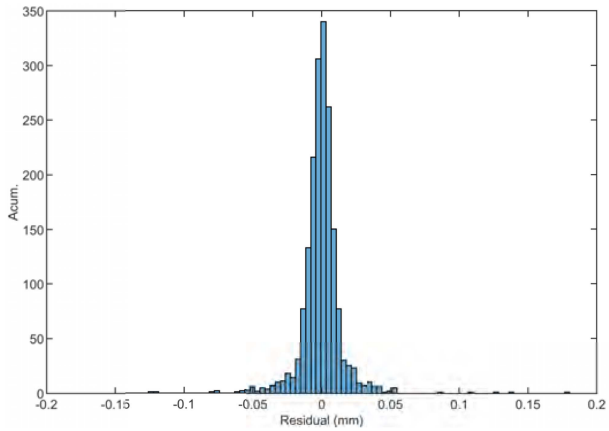

Fig. 20. Histogram of the differences between the mean deviation and the model at the center of the rail head for all repetitions.

can be found at the beginning and at the end of the rail. These sections are often removed before the rail is used.

In order to quantitatively assess the repeatability of the system, the difference between all profiles and the mean is calculated. This procedure provides a difference profile for each experiment. All these differences, or residuals, indicate the dispersion of the measurements. The distribution of all the residuals can be seen in the histogram shown in Fig. 20. To test the normality of the distribution of the residuals, the Shapiro-Wilk parametric hypothesis test of composite normality is used. This hypothesis test confirmed the normality of the distribution at 99.99% confidence. Therefore, the residuals can be considered to follow a normal distribution. Given this distribution, a confidence interval for the repeatability of the mean deviation is ± 0.001 mm, providing a level of confidence of approximately 99%.

IV. Conclusion

The characterization of surface topography is of utmost importance for quality control in product manufacturing. Features about regular and irregular patterns, roughness, waviness and dimensions are crucial to determining the properties of the final manufactured product. This work focuses on the measurement of flatness in rails. The proposed solution combines two triangulation units with cameras and laser projectors to extract a height profile with a cross-section of the rail. The sequence of profiles, acquired while the rail is moving forward, is accurately aligned with the model and the deviations of the surface from its intended shape are calculated. After filtering, the calculated quality control features ensure compliance with quality criteria. Thus, the proposed inspection system prevents failures and guarantees serviceability.

This work makes innovative contributions in different areas such as calibration, registration, calculation of deviations from the model and filtering. The result is a robust industrial application that can be used to accurately measure the flatness of rails. Results indicate the proposed inspection method provides excellent performance. The inspection system not only accurately calculates surface deviations from the intended shape, but can also function effectively with data contaminated by noise, as shown in tests. Additionally, the reliability of the quality control system is demonstrated by the repeatability experiments. The proposed approach provides important advantages regarding the simplification and optimization of rail flatness measurement systems, resulting in a more cost-effective and reliable solution for industrial applications. This new approach presents technical advancements and contributions compared with previous solutions.

The proposed procedures are designed to work in real-time with rail manufacturing. Therefore, products can be characterized online, which ensures they are being manufactured according to the specifications. In this way, the inspection system minimizes downtime and maximizes efficiency. Moreover, the proposed inspection approach is valid for any long product, where similar potential applications could be found.

REFERENCES

[1] R. Usamentiaga, F. Garcia, and D. F. delaCalle, "Rail flatness measurement based on dual laser triangulation," in *Proc. IEEE Ind. Appl. Soc. Conf.*, 2023, pp. 1–8.

[2] S. Ghorai, A. Mukherjee, M. Gangadaran, and P. K. Dutta, "Automatic defect detection on hot-rolled flat steel products," *IEEE Trans. Instrum. Meas.*, vol. 62, no. 3, pp. 612–621, Mar. 2013.

[3] J. Li et al., "Research on the measurement of the large-components flatness based on gravitational straightedge method of adaptive two-end growth," *Optik*, vol. 261, 2022, Art. no. 169139.

[4] *Railway Applications - Track Rail Part 1: Vignole Railway Rails 46 kg/m and Above*, Standard EN-13674-1, European Committee for for Standardization, Brussels, Belgium, Feb. 2011.

[5] R. Usamentiaga, D. F. Garcia, and F. J. de la Calle Herrero, "Real-time inspection of long steel products using 3D sensors: Calibration and registration," *IEEE Trans. Ind. Appl.*, vol. 54, no. 3, pp. 2955–2963, May/Jun. 2018.

[6] R. Usamentiaga, J. Molleda, and D. F. García, "Fast and robust laser stripe extraction for 3D reconstruction in industrial environments," *Mach. Vis. Appl.*, vol. 23, no. 1, pp. 179–196, 2012.

[7] R. Usamentiaga, J. Molleda, D. F. Garcia, F. G. Bulnes, J. Entrialgo, and C. M. S. Alvarez, "Flatness measurement using two laser stripes to remove the effects of vibrations," *IEEE Trans. Ind. Appl.*, vol. 51, no. 5, pp. 4297–4304, Sep./Oct. 2015.

[8] P. Manso, D. Garcia, and R. Usamentiaga, "A method to extract rail flatness profile and analysis of different noise sources," *IEEE Trans. Ind. Appl.*, vol. 58, no. 5, pp. 6801–6813, Sep./Oct. 2022.

[9] S. M. M. Gazafrudi, D. Younesian, and M. Torabi, "A high accuracy and high speed imaging and measurement system for rail corrugation inspection," *IEEE Trans. Ind. Electron.*, vol. 68, no. 9, pp. 8894–8903, Sep. 2021.

[10] D. Wei, X. Wei, Y. Liu, L. Jia, and W. Zhang, "The identification and assessment of rail corrugation based on computer vision," *Appl. Sci.*, vol. 9, no. 18, 2019, Art. no. 3913.

[11] L. Chen, Y. Li, X. Zhong, Q. Zheng, and H. Liu, "An automated system for position monitoring and correction of chord-based rail corrugation measuring points," *IEEE Trans. Instrum. Meas.*, vol. 68, no. 1, pp. 250–260, Jan. 2019.

[12] R. Hartley and A. Zisserman, *Multiple View Geometry in Computer Vision*. Cambridge, U.K.: Cambridge Univ. Press, 2003.

[13] J. Li and Z. Liu, "Efficient camera self-calibration method for remote sensing photogrammetry," *Opt. Exp.*, vol. 26, no. 11, pp. 14213–14231, 2018.

[14] K. Liao et al., "Deep learning for camera calibration and beyond: A survey," 2023, *arXiv:2303.10559*.

[15] J. Huo, Z. Meng, H. Zhang, S. Chen, and F. Yang, "Feature points extraction of defocused images using deep learning for camera calibration," *Measurement*, vol. 188, 2022, Art. no. 110563.

[16] Z. Zhang, "A flexible new technique for camera calibration," *IEEE Trans. Pattern Anal. Mach. Intell.*, vol. 22, no. 11, pp. 1330–1334, Nov. 2000.

[17] C. Steger, "An unbiased detector of curvilinear structures," *IEEE Trans. Pattern Anal. Mach. Intell.*, vol. 20, no. 2, pp. 113–125, Feb. 1998.

[18] J. Zhang, Y. Yao, and B. Deng, "Fast and robust iterative closest point," *IEEE Trans. Pattern Anal. Mach. Intell.*, vol. 44, no. 7, pp. 3450–3466, Jul. 2022.

[19] A. Myronenko and X. Song, "Point set registration: Coherent point drift," *IEEE Trans. Pattern Anal. Mach. Intell.*, vol. 32, no. 12, pp. 2262–2275, Dec. 2010.

[20] Z. Zhang, Y. Dai, and J. Sun, "Deep learning based point cloud registration: An overview," *Virtual Reality Intell. Hardware*, vol. 2, no. 3, pp. 222–246, 2020.

[21] R. Usamentiaga, D. F. García, and J. Molleda, "Efficient registration of 2D points to cad models for real-time applications," *J. Real-Time Image Process.*, vol. 15, no. 2, pp. 329–347, 2018.

[22] B. Muralikrishnan and J. Raja, *Computational Surface and Roundness Metrology*. Berlin, Germany: Springer, 2008.